Color version available online

Fig. 1. Intra-operative photograph of an eye with a rhegmatogenous RD which had DITC, i.e. the trocar cannula could not be inserted into the vitreous during 23-gauge MIVS. **a** The infusion cannula could not be inserted into the vitreous. **b** Vitreous gel is partially leaking into the infusion cannula which is incompletely inserted. **c** The gel was removed with the vitreous cutter, and the pars plana region was gently compressed. **d** The infusion cannula is completely inserted into the vitreous after counter assistance. This technique of counter assistance was performed for DITC.

There are three disadvantages of MIVS. First, there are cases where it is difficult to insert the 23- or 25-gauge microcannula [8]. Second, both the 23- and 25-gauge instruments can be jammed in the cannula by vitreal haemorrhage [9, 10]. And third, the 25-gauge soft-tip needle is unable to completely remove fluid during air-fluid exchange because the needle cannot reach the back of an elongated globe in highly myopic eyes [11]. The second and third problems are relatively easy to overcome from the pre-operative findings, and eyes with these properties can undergo conventional 20-gauge pars plana vitrectomy (PPV).

However, the cause for the difficulty in inserting the trocar cannula (DITC) into the vitreous has not been determined, and determining its cause is difficult because it is encountered only intra-operatively during MIVS but at a very low frequency. At present, it cannot be predicted by the pre-operative demographics which eyes will have DITC.

Thus, the purpose of this study was to determine the incidence of eyes in which DITC is encountered during MIVS, and to determine the pre-operative characteristics of eyes that are associated with this problem.

Patients and Methods

Subjects

We reviewed the medical records of 1,525 consecutive eyes that had undergone PPV with either a 25- or a 23-gauge trocar cannula system (table 1; Alcon Laboratories, Fort Worth, Tex., USA). Only eyes that had undergone MIVS performed by a single surgeon (H.K.) at the Surgical Retina Clinic of the Tohoku University Hospital from May 2006 to November 2009 were included. Eyes that had undergone 20-gauge PPV for complex vitreoretinal disease such as severe proliferative vitreoretinopathy and severe proliferative diabetic retinopathy were excluded.

After the purpose and procedures of the operation had been explained, an informed consent was obtained from all patients. The procedures used conformed to the tenets of the Declaration of Helsinki and this study was approved by the Review Board of the School of Medicine, Tohoku University.

Surgical Procedures

All surgeries were performed under retrobulbar anaesthesia using the oblique sclerotomy technique with the Accurus Vitrectomy System (Alcon Laboratories) [12]. The choice between 25- and 23-gauge MIVS was made by the surgeon (H.K.) based on the clinical findings of the eye. First, an infusion cannula was inserted through the inferotemporal sclera followed by the insertion of 2 cannulas through superotemporal and superonasal sites. The exact surgical procedures varied according to the type of retinal disease.

We defined a DITC as the condition where at least 1 trocar cannula could not be inserted into the vitreous at the beginning of MIVS.

Pre-Operative Measurements in Patients with RD

To determine the pre-operative factors that were associated with an intra-operative DITC, the intra-ocular pressure (IOP), refractive error, size of the RD and the presence of a choroidal detachment were investigated in patients with an RD. The IOP was measured with a non-contact tonometer or a Goldmann applanation tonometer, and the refractive error (diopters) was determined with an autorefractometer (Tonoref RKT-7700 or ARK-700; Nidek). The extent of the RD was graded from 1 to 4 according to the number of quadrants it covered. The presence of a pre-operative choroidal detachment was also recorded.

Technique of Counter Assistance for Eyes with DITC

We define the 'technique of counter assistance' as vitrector-assisted perforation of the pars plana. The vitreal cutter was relatively easy to insert into the vitreous through the superior site because the cutter was much longer than the infusion cannula. However, when the infusion cannula could not be inserted into the vitreous, i.e. in cases of DITC, the insertion was made possible by inserting the cannula using the vitreal cutter from the superior nasal side (fig. 1a). During this procedure, vitreous gel was leaking into the partially inserted infusion cannula (fig. 1b). The extra gel was cut and removed by the vitreous cutter, and the head of the cutter was gently pressed against the pars plana region that had been perforated by the infusion cannula from the outside of the eye (fig. 1c). Then, the infusion cannula was inserted into the vitreous and fixed (fig. 1d). In cases of DITC, we first tried the technique of counter assistance, and next converted to 20-gauge PPV if the technique was not successful.

Table 1. Incidence of DITC in 25- and 23-gauge MIVS

Surgical procedure	Incidence of DITC	Age, years	Disease and number of eyes
25-Gauge MIVS (n = 1,294)	5/1,294 (0.4%)[a]	4–93 (mean 62.6 ± 13.7)[b]	proliferative diabetic retinopathy (237, 18.3%)[c] epiretinal membrane (371, 28.7%) macular hole (153, 11.8%) RD (154, 11.9%) vitreous haemorrhage and opacity (76, 5.9%) proliferative vitreoretinopathy (56, 4.3%) macular oedema (184, 14.2%) ocular perforating injury (7, 0.5%) others (56, 4.3%)
23-Gauge MIVS (n = 231)	4/231 (1.7%)[a]	9–86 (mean 55.9 ± 16.8)[b]	proliferative diabetic retinopathy (55, 23.8%)[c] epiretinal membrane (3, 1.3%) macular hole (17, 7.4%) RD (88, 38.1%) vitreous haemorrhage and opacity (19, 8.2%) proliferative vitreoretinopathy (39, 16.9%) macular oedema (7, 3.0%) ocular perforating injury (1, 0.4%) others (2, 0.9%)

[a] $p = 0.0346$ (Fisher's exact probability test), [b] $p < 0.0001$ (Mann-Whitney test), [c] $p < 0.0001$ (χ^2 for independence test), 25- versus 23-gauge.

DITC Score

There were 4 factors that determined the possibility that DITC will be encountered during MIVS in eyes with RD, and eyes were graded by these factors: a total RD (4 quadrants), a choroidal detachment, myopia >-8.0 dpt (high myopia) and hypotony <8 mm Hg. The DITC score ranged from 0 to 4 according to the number of these factors that were present, and the DITC score of each eye was determined.

Statistical Analyses

The significance of the difference in the mean age of the patients who had undergone 25- and 23-gauge MIVS was determined by the Mann-Whitney U test. The significance of the difference in the incidence of DITC for cases that had 25-gauge MIVS and those that had 23-gauge MIVS was determined by Fisher's exact probability test. Non-DITC eyes with an RD which had had all of the data for the 4 factors and were phakic were compared with DITC eyes with RD using statistical packages including Mann-Whitney U test or Fisher's exact probability test. Eyes with dense vitreous haemorrhage or which were pseudophakic were excluded from the analysis to determine the possibility of DITC in eyes with RD because the original refractive error could not be determined. For the analyses of RD, in cases that had surgery on both eyes or had multiple surgeries on one eye, only one eye was used for the statistical analyses.

Results

Incidence of DITC during 25- and 23-Gauge MIVS

The incidence of DITC for all eyes was 0.6% (9 of 1,525 eyes; table 1). The incidence of DITC in eyes undergoing 23-gauge MIVS was 1.7% (4/231) which was significantly higher than the 0.4% (5/1,294) undergoing 25-gauge MIVS (p = 0.0346; Fisher's exact probability test). The mean age of the patients who had 25-gauge MIVS was 62.6 ± 13.7 years which was significantly higher than the 55.9 ± 16.8 years for those who had 23-gauge MIVS (p < 0.0001, Mann-Whitney test). The distribution of the different types of diseases was also statistically different in 25- and 23-gauge MIVS (p < 0.0001, χ^2 for independence test). Eyes with an epiretinal membrane that had 25-gauge MIVS were 22 times more frequent than eyes that had 23-gauge MIVS. For macular oedema, eyes that had 25-gauge MIVS were 4 times more frequent than eyes that had 23-gauge MIVS. Eyes with RD and proliferative vitreoretinopathy that had 23-gauge MIVS were 3 times more frequent than those which underwent 25-gauge MIVS.

Kunikata/Nitta/Meguro/Aizawa/Hariya/ Chiba/Abe/Nishida

Table 2. Clinical data of 9 eyes causing DITC in 25- or 23-gauge MIVS

Eye No.	Age years	Gender	Diagnosis	Gauge size	Pre-operative IOP, mm Hg	Refractive error, dpt	Choroidal detachment	Size of RD (1–4 quadrants)	Final treatment
1	74	M	OPI	25	–	–	–	–	converted to 20-gauge PPV
2	59	M	RRD	25	4	–0.125	yes	4	counter assistance
3	59	M	RRD	23	5	–0.125	no	4	converted to 20-gauge PPV
4	51	M	RRD	25	4	–10.0	yes	4	counter assistance
5	58	M	RRD	25	5	–2.25	yes	4	converted to 20-gauge PPV
6	59	F	RRD	25	9	–2.25	no	4	counter assistance
7	79	F	MHRD	23	5	–10.0	no	4	counter assistance
8	55	F	RRD	23	7	–10.8	yes	3	counter assistance
9	42	F	RRD	23	14	–8.50	no	4	converted to 20-gauge PPV

OPI = Ocular perforating injury; RRD = rhegmatogenous RD; MHRD = RD due to macular hole in high myopia.

Table 3. Characteristics of 167 eyes with RD: pre-operative IOP, refractive error, choroidal detachment and size of RD in MIVS with and without 25- and 23-gauge DITC

	Overall	No DITC	DITC	p value
Number of eyes	167	160	7	–
Mean age ± SD, years	57.7 ± 10.7	57.7 ± 10.7	57.6 ± 11.2	0.6547[1]
Sex, n				0.3749[2]
Male	93	90	3	
Female	74	70	4	
Gauge, n				0.4340[2]
25-gauge MIVS	111 (66.5)	107 (96.4)	4 (3.6)	
23-gauge MIVS	56 (33.5)	53 (94.6)	3 (5.4)	
Mean pre-operative IOP ± SD, mm Hg	12.1 ± 3.9	12.3 ± 3.7	6.9 ± 3.6	0.0016[1]
Hypotony (<8 mm Hg), n	20/167 (12.0)	15/160 (9.4)	5/7 (71.4)	0.0003[2]
Mean refractive error ± SD, dpt	–3.7 ± 4.7	–3.5 ± 4.7	–6.3 ± 4.5	0.1049[1]
High myopia (>–8 dpt), n	30/167 (18.0)	26/160 (12.5)	4/7 (57.1)	0.0204[2]
Choroidal detachment, n	5/167 (3.0)	1/160 (0.6)	4/7 (57.1)	<0.0001[2]
Mean size of RD ± SD				
(1–4 quadrants)	2.2 ± 0.9	2.1 ± 0.9	3.9 ± 0.4	<0.0001[1]
Total RD (4 quadrants), n	18/167 (10.8)	12/160 (7.5)	6/7 (85.7)	<0.0001[2]

Figures in parentheses indicate percentages. SD = Standard deviation. [1] Mann-Whitney test. [2] Fisher's exact probability test.

Characteristics of Eyes That Had DITC

There were 9 eyes of 8 patients with DITC (4 men and 4 women; table 2), and their mean age ± standard deviation was 59.6 ± 11.1 years (range, 42–79 years). Eight of the 9 eyes (88.9%) with DITC had an RD including a macular hole retinal detachment (MHRD). For all eyes, the number with an RD was 242, and the incidence of DITC in these eyes was 3.3% (8 of 242 eyes). The other eye with DITC had only had suturing surgery for an ocular perforating injury 1 week before, and a dense vitreous haemorrhage was still present at the time of surgery. In the 8 eyes with a pre-operative RD, 7 had a total RD, 4 also had a choroidal detachment, 4 also had high myopia (>–8.0 dpt), and 6 were also hypotonic (<8 mm Hg).

To counteract the DITC, we performed the counter assistance technique on 5 eyes, as described in the Patients and Methods section (fig. 1; table 2).

Table 4. Percentage of the incidence of 25- and 23-gauge DITC in the eyes with RD by hypotony, high myopia, choroidal detachment or total RD, and DITC score

	Overall n	No DITC n	DITC n	DITC %
Hypotony (<8 mm Hg)	20	15	5	25.0
High myopia (>–8 dpt)	30	26	4	13.3
Choroidal detachment	5	1	4	80.0
Total RD (4 quadrants)	18	12	6	33.3
DITC score				
0	113	113	0	0
1	41	40	1	2.4
2	8	7	1	12.5
3	4	0	4	100
4	1	0	1	100

Pre-Operative IOP, Refractive Error, Choroidal Detachment and Size of RD in Eyes with DITC

The pre-operative IOP, refractive error, choroidal detachment and size of the RD in the eyes undergoing MIVS for RD are shown in table 3. There were 8 eyes with an RD that had DITC and 1 had a recurrence of the RD (table 2, eyes No. 2 and 3). For the statistical analyses, we excluded eye No. 3 and used the remaining 7 eyes to compare the demographics to that of the 160 non-DITC eyes with an RD.

Pre-operatively, 6 of the 7 eyes had a total RD, 4 of 7 eyes also had a choroidal detachment, 4 of 7 eyes were also highly myopic (>–8.0 dpt), and 5 of 7 eyes were also hypotonic (<8 mm Hg). The mean IOP of the 7 DITC eyes with an RD was 6.9 ± 3.6 mm Hg which was significantly lower than that of non-DITC eyes at 12.3 ± 3.7 mm Hg (p = 0.0016 Mann-Whitney test). The percentage of eyes with DITC that were also hypotonic (<8 mm Hg) was 71.4% (5/7) which was significantly higher than that of non-DITC eyes which was 9.4% (15/160; p = 0.0003, Fisher's exact probability test).

The mean refractive error of the DITC eyes was –6.3 ± 4.5 dpt which was not significantly different from that of non-DITC eyes which was –3.5 ± 4.7 dpt (p = 0.1049; Mann-Whitney test). The percentage of eyes with DITC and also high myopia (>–8 dpt) was 57.1% (4/7), which was significantly higher than that of non-DITC eyes which was 12.5% (26/160; p = 0.0204; Fisher's exact probability test).

The percentage of eyes with DITC and also choroidal detachment was 57.1% (4/7), which was significantly

higher than that of non-DITC eyes which was 0.6% (1/160; p < 0.0001; Fisher's exact probability test). The mean size of the RD of DITC eyes was 3.9 ± 0.4 quadrants, which was significantly greater than that of the non-DITC eyes which was 2.1 ± 0.9 quadrants (p < 0.0001, Mann-Whitney test). The percentage of eyes with a total RD in the eyes with DITC was 85.7% (6/7), which was also significantly higher than that of non-DITC eyes which was 7.5% (12/160; p < 0.0001, Fisher's exact probability test).

Incidence of DITC in Eyes with Hypotony, High Myopia, Choroidal Detachment or Total RD, and DITC Score

The distribution of eyes with DITC and also hypotony, high myopia, a choroidal detachment or a total RD, and the DITC scores are shown in table 4. The incidence of DITC was 25.0% (5/20) in eyes with hypotony, 13.3% (4/30) in eyes with high myopia, 80.0% (4/5) in eyes with choroidal detachment and 33.3% (6/18) in eyes with a total RD. The incidence of eyes with a DITC score of 0 was 0% (0/113), 2.4% (1/41) in eyes with a DITC score of 1, 12.5% (1/8) in eyes with a DITC score of 2, 100% (4/4) in eyes with a DITC score of 3, and 100% (1/1) in eyes with a DITC score of 4.

Discussion

Our findings showed that the DITC cases were rare with an overall incidence of 0.6% (9 of 1,525 eyes). The cases of DITC were found to be associated with eyes with RD, hypotony, choroidal detachment and high myopia. We suggest that the DITC is associated with the balance between a resistance to insertion and the IOP. If this resistance is high because of the construction of the trocar or its dullness, then DITC may occur. If the material and shape of the trocar and sclera were all the same, i.e. same resistance to insertion, DITC would only occur in eyes with hypotony or a choroidal detachment due to suprachoroidal fluid. Thus, if the resistance to insertion was higher or IOP was low or suprachoroidal fluid existed, the DITC would most likely occur at the beginning of MIVS.

Eyes with severe or long-standing RD are often hypotonic and have choroidal detachment, so it is reasonable that the size of the RD was also significantly correlated with DITC as were hypotony and choroidal detachment. Although it is unclear how the high myopia was associated with DITC because a thin sclera should reduce the resistance to insertion, one explanation might be a pre-

Kunikata/Nitta/Meguro/Aizawa/Hariya/
Chiba/Abe/Nishida

disposition toward the development of hypotony and choroidal detachment [13].

Another reason for the DITC with both the 25- and 23-gauge instruments might be because the tip of the trocar is not slit-shaped but beveled. A microvitreoretinal (MVR) blade has been used to make a slit-shaped incision to make it easier for the trocar to penetrate the sclera and to enhance wound closure [14]. This MVR trocar was found to have a lower resistance to insertion than that of the conventional trocar cannula with a beveled needle trocar [14]. So, the new MIVS trocar cannula with an MVR blade might decrease the incidence of DITC. However, we believe that 20-gauge PPV is still a useful system for eyes with the 4 ocular risk factors.

Suprachoroidal fluid effuses during conventional 20-gauge PPV when the 20-gauge MVR blade is pulled out from the sclera which usually collapses the choroidal detachment. The 20-gauge instruments have not only a 4-mm infusion cannula but also a 6-mm infusion cannula which can perforate the sclera and choroid more easily. On the other hand, suprachoroidal fluid cannot effuse from the trocar cannula of the 23- and 25-gauge instruments, although suprachoroidal fluid has been demonstrated to also be a complication of 23-gauge MIVS [15].

The incidence of DITC with 23-gauge instruments was significantly higher than that with 25-gauge instruments. The trocar cannula of the 23-gauge system has been reported to have some difficulties in creating scleral ports including the presence of suprachoroidal fluid as an intra-operative complication and hypotony as a postoperative complication after 23-gauge MIVS [15–19]. However, we cannot simply compare the result of 25-gauge MIVS with that of 23-gauge MIVS. Because, for the surgeon's preference, we performed 23-gauge MIVS more often for complicated cases such as RD or proliferative vitreoretinopathy but not for macular diseases such as macular oedema or epiretinal membrane.

The pre-operative presence of a choroidal detachment was the greatest risk factor for DITC (4/5, 80.0%; table 4) in our cases, although choroidal detachment was not often present in eyes with an RD. The DITC score was also a good index to predict the occurrence of DITC during MIVS for eyes with an RD because scores ≥ 3 indicated that the incidence of DITC would be 100%. In addition, DITC is rarely (1/154, 0.6%) found in eyes with a DITC score of ≤ 1. This is important because it was then not necessary to consider DITC if only 1 or none of the 4 risk factors was present. Although performing MIVS is possible in eyes with a DITC score of 0 and 1, an alternative plan of 20-gauge PPV might be recommended with DITC

scores of 2–4. Considering the 4 eyes in which MIVS was finally switched to 20-gauge PPV because we could easily create the 20-gauge ports even for such cases, it is recommended that 20-gauge PPV should be used first for the eyes which have multiple risk factors, i.e. those with DITC scores of ≥ 2.

The diseases which had DITC during MIVS were eyes with rhegmatogenous RD, MHRD and after initial surgery for an ocular perforation. So, eyes with other vitreoretinal diseases will probably not have DITC during MIVS. However, we believe that hypotony might be critical and lead to a DITC even in eyes without an RD, choroidal detachment and the conditions after the initial surgery for an ocular perforation. MHRD has also been reported to create a predisposition toward hypotony and choroidal detachment [13]. The MHRD is the reason why these patients do not have good vision. So, although there was only 1 eye with an MHRD in our series, it had DITC. We believe that MHRD might be the one condition that has the highest potential for DITC.

Our study has several weaknesses, including the retrospective aspect with no controls and surgeries by only one surgeon. However, because the DITC frequently happened at the beginning of MIVS, it is valuable to evaluate the incidence of DITC as it is related to different pre-operative ocular conditions without considering the experience of different surgeons.

Our findings indicated that DITC during MIVS occurs mainly in patients with RD. A large area of RD, choroidal detachment, high myopia and hypotony were significant risk factors for DITC in eyes with an RD. We recommend that MIVS should be performed cautiously for patients with these risk factors.

Acknowledgements

Disclosure Statement

Proprietary interests, none.

References

1 Fujii GY, De Juan E Jr, Humayun MS, et al: A new 25-gauge instrument system for transconjunctival sutureless vitrectomy surgery. Ophthalmology 2002;109:1807–1812, discussion 1813.
2 Fujii GY, De Juan E Jr, Humayun MS, et al: Initial experience using the transconjunctival sutureless vitrectomy system for vitreoretinal surgery. Ophthalmology 2002;109: 1814–1820.
3 Eckardt C: Transconjunctival sutureless 23-gauge vitrectomy. Retina 2005;25:208–211.
4 Kellner L, Wimpissinger B, Stolba U, Brannath W, Binder S: 25- vs 20-gauge system for pars plana vitrectomy: a prospective randomised clinical trial. Br J Ophthalmol 2007; 91:945–948.
5 Tsang CW, Cheung BT, Lam RF, et al: Primary 23-gauge transconjunctival sutureless vitrectomy for rhegmatogenous retinal detachment. Retina 2008;28:1075–1081.
6 Mura M, Tan SH, De Smet MD: Use of 25-gauge vitrectomy in the management of primary rhegmatogenous retinal detachment. Retina 2009;29:1299–1304.
7 Kunikata H, Nishida K: Visual outcome and complications of 25-gauge vitrectomy for rhegmatogenous retinal detachment: eighty-four consecutive cases. Eye 2010;24:1071–1077.
8 Byeon SH, Chu YK, Lee SC, Koh HJ, Kim SS, Kwon OW: Problems associated with the 25-gauge transconjunctival sutureless vitrectomy system during and after surgery. Ophthalmologica 2006;220:259–265.
9 Shinoda H, Nakajima T, Shinoda K, Suzuki K, Ishida S, Inoue M: Jamming of 25-gauge instruments in the cannula during vitrectomy for vitreous haemorrhage. Acta Ophthalmol 2008;86:160–164.
10 Nam DH, Ku M, Sohn HJ, Lee DY: Jamming of 23-gauge instruments in the microcannula during vitrectomy for severe vitreous haemorrhage. Acta Ophthalmol 2010;88: e134–e135.
11 Singh A, Fawzi AA, Stewart JM: Limitation of 25-gauge vitrectomy instrumentation in highly myopic eyes. Ophthalmic Surg Lasers Imaging 2007;38:437–438.
12 Shimada H, Nakashizuka H, Mori R, Mizutani Y, Hattori T: 25-Gauge scleral tunnel transconjunctival vitrectomy. Am J Ophthalmol 2006;142:871–873.
13 Kang JH, Park KA, Shin WJ, Kang SW: Macular hole as a risk factor of choroidal detachment in rhegmatogenous retinal detachment. Korean J Ophthalmol 2008;22:100–103.
14 Inoue M, Shinoda K, Shinoda H, Suzuki K, Kawamura R, Ishida S: 25-Gauge cannula system with microvitreoretinal blade trocar. Am J Ophthalmol 2007;144:302–304.
15 Ooto S, Kimura D, Itoi K, et al: Suprachoroidal fluid as a complication of 23-gauge vitreous surgery. Br J Ophthalmol 2008;92:1433–1434.
16 Gupta OP, Ho AC, Kaiser PK, et al: Short-term outcomes of 23-gauge pars plana vitrectomy. Am J Ophthalmol 2008;146:193–197.
17 Fine HF, Iranmanesh R, Iturralde D, Spaide RF: Outcomes of 77 consecutive cases of 23-gauge transconjunctival vitrectomy surgery for posterior segment disease. Ophthalmology 2007;114:1197–1200.
18 Woo SJ, Park KH, Hwang JM, Kim JH, Yu YS, Chung H: Risk factors associated with sclerotomy leakage and postoperative hypotony after 23-gauge transconjunctival sutureless vitrectomy. Retina 2009;29:456–463.
19 Haas A, Seidel G, Steinbrugger I, et al: Twenty-three-gauge and 20-gauge vitrectomy in epiretinal membrane surgery. Retina 2010; 30:112–116.

Successful Outcomes of 25- and 23-Gauge Vitrectomies for Giant Retinal Tear Detachments

Hiroshi Kunikata, MD, PhD; Toshiaki Abe, MD, PhD; Kohji Nishida, MD, PhD

■ **BACKGROUND AND OBJECTIVE:** The authors examined the feasibility of performing 25- and 23-gauge micro-incision vitrectomy surgery (MIVS) for a giant retinal tear.

■ **PATIENTS AND METHODS:** The medical records of 12 eyes of 11 patients with giant retinal tear who underwent MIVS using perfluorocarbon liquids were reviewed. All patients were observed for at least 6 months postoperatively.

■ **RESULTS:** An intraoperative re-attachment was achieved in 12 eyes (100%) and 11 eyes (92%) remained attached without intraocular tamponade. Sili-cone oil was used in 9 of 12 eyes and removed 2 weeks after the initial vitrectomy except in one eye. The postoperative retinal complications included macular pucker in two eyes, subretinal perfluorocarbon liquid in two eyes, retinal folds in one eye, cystoid macular edema in one eye, and redetachment due to proliferative vitreoretinopathy in one eye.

■ **CONCLUSION:** Although the study had a short follow-up period, primary MIVS appears to be safe and feasible for giant retinal tear surgery.

[Ophthalmic Surg Lasers Imaging 201X;XX:XX-XX.]

INTRODUCTION

A retinal detachment with a giant retinal tear (≥ 90°) is difficult to treat successfully for even experienced vitreous surgeons. There have been different treatments for giant retinal tears, including pneumatic retinopexy, wide scleral buckling, and conventional 20-gauge pars plana vitrectomy (PPV) with gas or silicone oil tamponade using perfluorocarbon liquid (PFCL). Management using PFCL increased the successful reattachment rate from approximately 40% to 80%.[1-8]

The use of 25- and 23-gauge micro-incision vitrectomy (MIVS) was first reported in 2002 and 2005, respec-

TABLE

Characteristics, Operative Details, and Postoperative Course of 12 Eyes With GRTs After Micro-incision Vitrectomy Surgery

Eye	Age (Y)	Lens Status	GRT (Degree)	GRT Location	G	Triple Surgery	Operative Time (Min)	SO	Decimal Pre VA	Decimal Final VA	Final Success	Postop Complications	FU (Mo)
1	15	Phakic	150	ST	25	N	71	N	0.1	0.7	Y	Pucker	39
2	26	Phakic	90	ST	25	Y	84	N	0.15	0.09	Y	N	6
3	26	Phakic	135	ST	25	Y	86	N	0.06	0.7	Y	RFs, SubPFCL	6
4	61	Phakic	150	S	25	Y	98	Y	0.7	1.0	Y	N	12
5	60	Phakic	120	ST	23	Y	75	Y	0.02	0.5	Y	N	24
6	60	Phakic	90	ST	23	Y	53	Y	1.0	1.0	Y	N	12
7	44	Phakic	150	S	23	Y	66	Y	HM	0.09	Y	PVR	12
8	35	IOL	150	T	23	N	119	Y	0.03	0.05	N	N	12
9	51	IOL	90	N	23	N	76	Y	1.0	1.0	Y	N	6
10	60	Phakic	120	I	23	Y	86	Y	CF	0.3	Y	SubPFCL	6
11	35	Phakic	90	T	23	Y	76	Y	0.4	0.1	Y	Pucker	6
12	45	IOL	135	T	25	N	41	Y	0.7	1.0	Y	CME	6

GRT = giant retinal tear; G = gauge; SO = silicone oil; pre = preoperative; VA = visual acuity; postop = postoperative; FU = follow-up; ST = superotemporal; RFs = retinal folds; SubPFCL = subretinal perfluorocarbon liquid; S = superior; HM = hand motions; IOL = intraocular lens; T = temporal; PVR = proliferative vitreoretinopathy; N = nasal; I = inferotemporal; CF = counting fingers; CME = cystoid macular edema.

tively.[9-11] These techniques have become commonly used throughout the world. The increase in popularity of MIVS was enhanced by the clinical studies demonstrating significant reductions in conjunctival injection and postoperative pain and discomfort. Despite the increased indications for MIVS for rhegmatogenous retinal detachments and the recent advances in giant retinal tear repair using PFCL, there are no publications on case series of giant retinal tear treated by MIVS.[12-18]

Thus, the purpose of this study was to determine the visual outcome and retinal complications of 12 consecutive eyes with a giant retinal tear treated by MIVS by a single surgeon.

PATIENTS AND METHODS

We reviewed the medical records of 12 eyes of 11 consecutive patients with a giant retinal tear (Table) who had undergone MIVS by one surgeon with either a 25- or a 23-gauge trocar cannula (Alcon Laboratories, Inc., Fort Worth, TX). The preoperative demographics of the patients are shown in the table. All of the surgeries were performed at the Surgical Retina Clinic of the Tohoku University Hospital between August 2007 and July 2010. The inclusion criteria were retinal detachment with a giant retinal tear of 90° or greater and treated by a single surgeon (HK). The exclusion criteria were prior vitrectomy and trauma.

After the purpose and procedures of the operation were explained, an informed consent was obtained from all patients. The procedures used conformed to the tenets of the Declaration of Helsinki and this study was approved by the Review Board of the School of Medicine, Tohoku University.

All surgeries were performed under retrobulbar anesthesia. A conjunctival peritomy was not made in all cases, and all surgeries were performed using the Accurus Vitrectomy System (Alcon Laboratories, Inc.). The crystalline lenses were extracted from all patients except one, who was a teenager. After resecting the vitreal core, the peripheral vitreous was shaved as much as possible. After the shaving, PFCL was injected on the disc and the vitreous cavity was filled with PFCL. Finally, endophotocoagulation was performed around all retinal tears. Silicone oil, sulfur hexafluoride, or perfluoropropane was used for intraocular tamponade. Antibiotics and corticosteroids were injected subconjunctivally in all cases postoperatively.
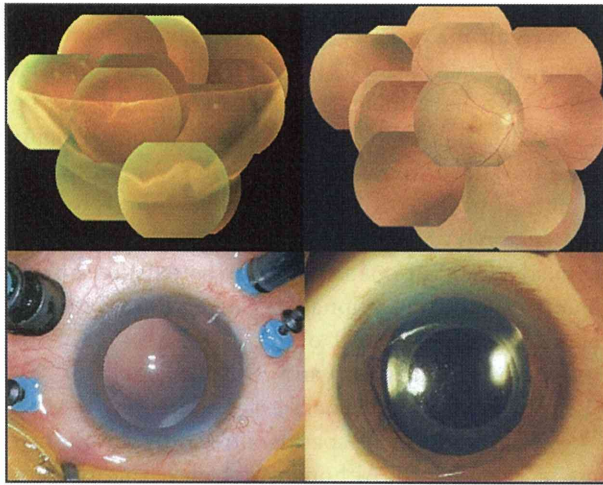
Figure. Representative eye with a giant retinal tear (GRT). Fundus and intraoperative photograph of the eye of a 61-year-old man (eye 4) with a retinal detachment from a GRT. The eye had undergone 25-gauge vitrectomy. (Upper left) Preoperative photograph of the right fundus showing a 150° GRT. (Upper right) Postoperative photograph of the right fundus showing complete re-attachment of the retina. (Lower left) Intraoperative photograph of 25-gauge ports for the infusion, chandelier light pipe, and cutter. The ports are placed in the inferotemporal, inferonasal, superonasal, and superotemporal quadrants. The superotemporal port was created at the lower side than adjusted to perform endophotocoagulation easily for the GRT. (Lower right) Photograph of the ocular surface 2 weeks postoperatively. The ocular surface is smooth with no subconjunctival hemorrhage and no conjunctival injection.

The outcome measures were the initial anatomical success rate, final anatomical success rate, postoperative visual acuity, and intraoperative and postoperative complications. The anatomical success after the initial surgery was defined as a complete reattachment of the retina after the silicone oil had been removed or all gas in the eye had disappeared. All of the patients had a complete ophthalmological examination at 6 months or more after the surgery. The final anatomical success was defined as a complete reattachment without intraocular tamponade at 6 months after the primary surgery.

The best-corrected visual acuity (BCVA) was measured using the Landolt C visual acuity chart, and the decimal acuities were converted to logarithm of the minimum angle of resolution (LogMAR) units. For statistical analyses, counting fingers visual acuity was set to 2.0 LogMAR units and hand motions visual acuity was set to 3.0 LogMAR units as used previously.[19,20] The preoperative and postoperative visual acuities were analyzed using statistical packages including Wilcoxon signed-rank test and Spearman's correlation coefficient by rank test.

RESULTS

The preoperative, intraoperative, and postoperative findings are summarized in the table. There were 9 men and 2 women whose mean ± standard deviation age at surgery was 43 ± 15 years. Their preoperative decimal BCVA ranged from hand motions to 1.0. The mean total operative time was 78 ± 19 minutes. We performed 25-gauge MIVS in 5 eyes and 23-gauge MIVS in 7 eyes. Triple surgery (phacoemulsification and aspiration, intraocular lens implantation, and MIVS) was performed on 8 eyes (67%). Only MIVS was performed on 4 eyes (33%) because 3 eyes had already undergone cataract surgery and the other eye belonged to a 15 year old with a clear lens. PFCLs were used in all 12 eyes.

We used 25-gauge MIVS in the first four cases with giant retinal tears (Table and Figure) and did not inject silicone oil in the first three cases. However, the third case had a postoperative retinal slippage and retinal folds but the retina remained attached during the follow-up period. Thereafter, we used silicone oil in all cases with a giant retinal tear to avoid retinal slippage and attained complete retinal attachment. We could not inject silicone oil through the 25-gauge cannula in the fourth case, and we switched to 23-gauge instruments in the subsequent cases so that silicone oil could be injected into the vitreous cavity. In the final case (eye 12), we used a new 25-gauge system that allowed us to inject silicone oil through the 25-gauge cannula. Silicone oil was used in the latter 9 of 12 eyes and removed 2 weeks after the initial vitrectomy, excluding one eye (eye 8) that developed proliferative vitreoretinopathy (PVR). None of our cases using silicone oil developed glaucoma requiring trabeculectomy.

An intraoperative reattachment was achieved in 12 eyes (100%) and 11 eyes (92%) remained attached at the last follow-up examination. The mean follow-up period was 12 ± 10 months with a range of 6 to 39 months.

The mean final BCVA was 0.46 ± 0.48 LogMAR units, which was better than the preoperative BCVA of 0.99 ± 0.90 LogMAR units but not significant ($P = .053$, Wilcoxon signed-rank test). The postoperative BCVA was significantly correlated with the preoperative BCVA ($P = .01$, Spearman's correlation coefficient by rank). The BCVA in 8 of the 12 eyes (67%) improved by more than 0.15 LogMAR units, and the visual improvement was significantly correlated with the preoperative VA (P

= 0.001; Spearman's correlation coefficient by rank test) for all 12 eyes. A final decimal BCVA of 0.5 or better was obtained in 7 of the 12 eyes (58%).

Six of the eyes developed retinal complications (50%); two eyes had a postoperative macular pucker needing additional surgery (17%), two eyes had a retention of subretinal PFCL (17%), one eye developed retinal folds (8%), one eye had cystoid macular edema (8%), and one eye had a redetachment of the retina due to PVR (8%). One of the two eyes with a macular pucker was treated surgically several months after the first operation and the pucker was completely removed (eye 1). Another eye with a macular pucker was also treated surgically several months after two vitreous surgeries (first vitrectomy to obtain a reattachment and second vitrectomy to remove the silicone oil) and the pucker was completely removed (eye 11). In the two eyes with a retention of subretinal PFCL, the PFCL was located in the posterior pole but not at the fovea, and the subretinal PFCL was removed completely in one eye when the silicone oil was removed (eye 10). In the other case, consent was not obtained from the patient (eye 3). The eye with the retinal folds was also not treated because of the good decimal BCVA of 0.7 and the lack of consent (eye 3). The eye with a postoperative cystoid macular edema was treated with posterior sub-Tenon injection of triamcinolone acetonide and the cystoid macular edema resolved (eye 12). The redetachment of the eye was treated surgically and reattachment was obtained with silicone oil tamponade (eye 8). However, the silicone oil in the case could not be removed because of hypotony during the follow-up period.

DISCUSSION

The highest primary success rate for giant retinal tear treated by 20-gauge PPV was that of Chang et al., who first introduced 20-gauge PPV using PFCL without scleral buckling in 1989.[6] Their rate was 94% with a minimum follow-up period of 6 months. Thus, the use of 20-gauge PPV to treat giant retinal tear has made the reattachment rate high using PFCL without buckling.[21] However, because the giant retinal tear is still difficult to treat, most ophthalmological institutes report primary success rates of approximately 70%. With additional surgeries, the highest success rate was better than 90%.[22,23] Although there are no reports of case series of giant retinal tear treated with MIVS, we

achieved an anatomical success rate of more than 90% after the initial surgery with MIVS, which suggests that even MIVS has similar results as reported by Chang et al.[6] Although the follow-up period in our patients was 6 months or more with a mean of 12 months, the number of treated patients was sufficient for us to conclude that MIVS as a primary surgery for giant retinal tear had better but not significantly better success rates than that with conventional 20-gauge PPV as reported recently by Lee et al.[1] (71 of 99, 71.7%; P = .12, Fisher's exact probability test) and Al-Khairi et al.[23] (92 of 117, 78.6%; P = .26, Fisher's exact probability test).

We performed lens-sparing vitrectomy for our first case (a 15 year old). Although we believe that the lens might become cataractous postoperatively in most patients after multiple vitreous surgeries, the lens of the first case that underwent two vitreous surgeries did not progress to cataract during the 3 years of follow-up. To remove the peripheral vitreous completely, lens-sparing vitrectomy might also be possible for eyes with giant retinal tear using a wide viewing system. However, the lens of patients older than 50 years or those with opacities should be removed during the initial vitrectomy.

In our 12 eyes, a reattachment was obtained after the initial MIVS in 11 eyes (92%) but subsequent surgery was necessary in 10 eyes (83%), including silicone oil removal 2 weeks after the initial vitrectomy in 8 eyes (67%), macular pucker removal in two eyes (17%), and surgery for a redetachment due to PVR in one eye (8%). Kertes et al. reported that 12 (7.4%) of their 162 patients who had undergone 20-gauge PPV with PFCL for giant retinal tear developed a macular pucker.[7] We found that two (17%) of the eyes developed a macular pucker needing additional surgery, which is slightly high but comparable to that reported by Kertes et al. (P = .24, Fisher's exact probability test).[7] The other postoperative complications of subretinal PFCL, retinal folds, and PVR have been reported to be 2 of 12 (16.7%),[1] 24 of 212 (11.3%),[8] and 10 of 128 (7.8%)[24] for conventional 20-gauge PPV in eyes with giant retinal tear. These rates are also not significantly different from ours (P = .71, .60, and .64, respectively, Fisher's exact probability test).

Our findings indicate that the advantages of MIVS for giant retinal tear are high rates of retinal attachment after the initial surgery, ease of injecting silicone oil, and comparable rates of postoperative retinal complications. However, there are limitations of using MIVS

4

for giant retinal tear. For example, the number of surgical instruments is limited and a greater requirement for wide angle viewing systems is needed.

Although there is no perfectly safe procedure for giant retinal tear, we recommend that eyes with a giant retinal tear should first undergo 23-gauge MIVS. We also recommend a silicone oil tamponade with 23-gauge MIVS to treat complex retinal detachments as reported.[13] However, 25-gauge MIVS with silicone oil tamponade was also reported to be efficient and can be considered in the surgical management of complex vitreoretinal disease.[14] Although we used the new 25-gauge system on only one case (eye 12), we believe that it can be as useful as the 23-gauge system. However, further investigations are needed to determine whether it is best to use the 25-gauge system for giant retinal tear.

Our technique required two vitreous surgeries (vitrectomy to obtain a reattachment and to inject silicone oil tamponade and surgery to remove the silicone oil). We removed the silicone oil 2 weeks after the primary MIVS if a reattachment developed because intraocular silicone oil can lead to postoperative complications such as glaucoma or PVR. We believe that a scarring adhesion between the retina and retinal pigment epithelium layer can develop within 2 weeks after photocoagulation.

In principle, we do not use an encircling buckle combined with primary MIVS for giant retinal tear, although the absence of an encircling scleral buckle was reported to be significantly associated with redetachment after 20-gauge PPV.[22,23] Further investigations are needed to determine whether an encircling buckle should be combined with MIVS for giant retinal tears. However, we believe that an encircling buckle should be combined with MIVS for giant retinal tears with other severe conditions such as PVR or those associated with severe atopic dermatitis. Even if an encircling buckle is used in combination with PPV, we believe that MIVS is more suitable than 20-gauge PPV because MIVS has the original advantage of having a cannula, which protects the sclerotomy port and might reduce occurrence of intraoperative iatrogenic retinal breaks.[25-27]

A comparison of visual acuities after PPV by conventional 20-gauge PPV and by MIVS is needed to assess the efficacy of MIVS on the final visual prognosis. Our study has limitations, including the short follow-up period, small number of patients, and surgery performed by a single surgeon. The number of patients is small be-cause giant retinal tear is a rare disease. Nevertheless, our findings indicate that MIVS is a feasible method and can lead to comparable retinal reattachment rates. In addition, because there are patients who develop a redetachment a few years after 20-gauge PPV, a follow-up of several years is recommended after MIVS.

REFERENCES

1. Lee SY, Ong SG, Wong DW, Ang CL. Giant retinal tear management: an Asian experience. *Eye (Lond).* 2009;23:601-605.
2. Schepens CL, Freeman HM. Current management of giant retinal breaks. *Trans Am Acad Ophthalmol Otolaryngol.* 1967;71:474-487.
3. Machemer R, Allen AW. Retinal tears 180 degrees and greater: management with vitrectomy and intravitreal gas. *Arch Ophthalmol.* 1976;94:1340-1346.
4. Norton EW, Aaberg T, Fung W, Curtin VT. Giant retinal tears: I. Clinical management with intravitreal air. *Trans Am Ophthalmol Soc.* 1969;67:374-393.
5. Leaver PK, Lean JS. Management of giant retinal tears using vitrectomy and silicone oil/fluid exchange: a preliminary report. *Trans Ophthalmol Soc U K.* 1981;101:189-191.
6. Chang S, Lincoff H, Zimmerman NJ, Fuchs W. Giant retinal tears: surgical techniques and results using perfluorocarbon liquids. *Arch Ophthalmol.* 1989;107:761-766.
7. Kertes PJ, Wafapoor H, Peyman GA, Calixto N Jr, Thompson H. The management of giant retinal tears using perfluoroperhydrophenanthrene: a multicenter case series. Vitreon Collaborative Study Group. *Ophthalmology.* 1997;104:1159-1165.
8. Scott IU, Murray TG, Flynn HW Jr, Feuer WJ, Schiffman JC. Outcomes and complications associated with giant retinal tear management using perfluoro-n-octane. *Ophthalmology.* 2002;109:1828-1833.
9. Fujii GY, De Juan E Jr, Humayun MS, et al. A new 25-gauge instrument system for transconjunctival sutureless vitrectomy surgery. *Ophthalmology.* 2002;109:1807-1812.
10. Fujii GY, De Juan E Jr, Humayun MS, et al. Initial experience using the transconjunctival sutureless vitrectomy system for vitreoretinal surgery. *Ophthalmology.* 2002;109:1814-1820.
11. Eckardt C. Transconjunctival sutureless 23-gauge vitrectomy. *Retina.* 2005;25:208-211.
12. Shimada H, Nakashizuka H, Mori R, Mizutani Y. Expanded indications for 25-gauge transconjunctival vitrectomy. *Jpn J Ophthalmol.* 2005;49:397-401.
13. Oliveira LB, Reis PA. Silicone oil tamponade in 23-gauge transconjunctival sutureless vitrectomy. *Retina.* 2007;27:1054-1058.
14. Riemann CD, Miller DM, Foster RE, Petersen MR. Outcomes of transconjunctival sutureless 25-gauge vitrectomy with silicone oil infusion. *Retina.* 2007;27:296-303.
15. Tsang CW, Cheung BT, Lam RF, et al. Primary 23-gauge transconjunctival sutureless vitrectomy for rhegmatogenous retinal detachment. *Retina.* 2008;28:1075-1081.
16. Von Fricken MA, Kunjukunju N, Weber C, Ko G. 25-Gauge sutureless vitrectomy versus 20-gauge vitrectomy for the repair of primary rhegmatogenous retinal detachment. *Retina.* 2009;29:444-450.
17. Mura M, Tan SH, De Smet MD. Use of 25-gauge vitrectomy in the management of primary rhegmatogenous retinal detachment. *Retina.* 2009;29:1299-1304.
18. Kunikata H, Nishida K. Visual outcome and complications of 25-G vitrectomy for rhegmatogenous retinal detachment: 84 consecutive cases. *Eye (Lond).* 2010;24:1071-1077.
19. Holladay JT. Proper method for calculating average visual acuity. *J Refract Surg.* 1997;13:388-391.
20. Mendrinos E, Dang-Burgener NP, Stangos AN, Sommerhalder J, Pournaras CJ. Primary vitrectomy without scleral buckling for pseudophakic rhegmatogenous retinal detachment. *Am J Ophthalmol.*

2008;145:1063-1070.

21. Ambresin A, Wolfensberger TJ, Bovey EH. Management of giant retinal tears with vitrectomy, internal tamponade, and peripheral 360 degrees retinal photocoagulation. *Retina.* 2003;23:622-628.

22. Goezinne F, Lah EC, Berendschot TT, et al. Low redetachment rate due to encircling scleral buckle in giant retinal tears treated with vitrectomy and silicone oil. *Retina.* 2008;28:485-492.

23. Al-Khairi AM, Al-Kahtani E, Kangave D, Abu El-Asrar AM. Prognostic factors associated with outcomes after giant retinal tear management using perfluorocarbon liquids. *Eur J Ophthalmol.* 2008;18:270-277.

24. Garcia-Valenzuela E, Ito Y, Abrams GW. Risk factors for retention of subretinal perfluorocarbon liquid in vitreoretinal surgery. *Retina.* 2004;24:746-752.

25. Fan WY, Xu J, Hou ZJ, Liu NP. Risk factors and prognosis of peripheral retinal breaks complicating pars plana vitrectomy [article in Chinese]. *Zhonghua Yan Ke Za Zhi.* 2008;44:776-779.

26. Rola A, Bailez Fidalgo C, Pastor Jimeno JC, et al. Iatrogenic retinal breaks during vitrectomy: retrospective study [article in Spanish]. *Arch Soc Esp Oftalmol.* 2003;78:487-491.

27. Carter JB, Michels RG, Glaser BM, De Bustros S. Iatrogenic retinal breaks complicating pars plana vitrectomy. *Ophthalmology.* 1990;97:848-853.

Energy & Environmental Science

Dynamic Article Links ▶

PAPER

Enzymatic biofuel cells designed for direct power generation from biofluids in living organisms†

Takeo Miyake,[ab] Keigo Haneda,[a] Nobuhiro Nagai,[c] Yohei Yatagawa,[a] Hideyuki Onami,[c] Syuhei Yoshino,[a] Toshiaki Abe[c] and Matsuhiko Nishizawa*[ab]

Enzymatic biofuel cells have attracted much attention for their potential to directly use biochemical energy sources in living organisms such as animals, fruits, *etc.* However, generally natural organisms have a skin, and the oxygen concentration in the organisms is lower than that of biofuels like sugars. Here, we fabricated a novel miniature assembly that consists of a needle bioanode for accessing biofuels in organisms through their skins and a gas-diffusion biocathode for utilizing the abundant oxygen in air. The performance of the biocathode was fourfold improved by optimizing its hydrophobicity. The assembled device with four needle anodes for fructose oxidation was inserted into a raw grape, producing a maximum power of 26.5 μW (115 μW cm^{-2}) at 0.34 V. A light-emitting diode (LED) with the cell served as a self-powered indicator of the sugar level in the grape. Power generation from blood sugar was also investigated by inserting a needle anode for glucose oxidation into a blood vessel in a rabbit ear. Prior coating of the tip of the needle anode with an anti-biofouling agent was effective to stabilize the output power.

Introduction

An enzymatic biofuel cell is a type of fuel cell where enzymatic catalysts are used to convert the chemical energy of biological fuels into electricity, instead of the metallic catalysts commonly used in fuel cells.[1–9] The high reaction selectivity of enzymes results in unique advantages, including the possibility of power

[a]Department of Bioengineering and Robotics, Tohoku University, 6-6-1 Aramaki Aoba, Aoba-ku, Sendai, 980-8579, Japan. E-mail: nishizawa@biomems.mech.tohoku.ac.jp; Tel: +81 22 795 7003
[b]Core Research for Evolutional Science and Technology (CREST), Japan Science and Technology Agency, Tokyo, 102-0075, Japan
[c]Division of Clinical Cell Therapy, United Centers for Advanced Research and Translational Medicine (ART), Graduate School of Medicine, Tohoku University, 2-1 Seiryo-machi, Aoba-ku, Sendai, 980-8575, Japan
† Electronic supplementary information (ESI) available: See DOI: 10.1039/c1ee02200h

generation from biofluids such as juices and bloods without purification. For example, Dong *et al.* have reported the energy-harvesting from natural fruit juices.[10,11] Furthermore, Mano *et al.* have demonstrated direct power generation in a grape berry using a glucose oxidase (GOD)-modified fine anode and a bilirubin oxidase (BOD)-modified fine cathode; both are inserted into a peeled grape.[12]

In the present investigation, we attempt to develop a miniature insertion device for energy harvesting from living organisms without any pretreatments. Such a device entails the following considerations. (1) Natural organisms are generally covered by a skin. (2) Oxygen in the organism is limited to a lower concentration than sugars.[13,14] (3) Biofluids contain reaction inhibitors for cathodic enzymes, such as ascorbic acid[15] and urate.[16,17] (4) Blood will form a clot on the surface of inserts. In order to address these considerations, our present device has been designed as shown in Fig. 1, which consists of a needle

Broader context

Power generation from the carbohydrates and alcohols produced by living systems is an attractive potential green energy technology, and has motivated for decades the development of enzymatic biofuel cells that can directly generate electricity without purification of the biofluids. In this study, we fabricated miniature biofuel cells that consist of a needle bioanode for accessing biofuels in organisms and a gas-diffusion biocathode for utilizing the abundant oxygen present in air. By inserting the needle into a grape, a light-emitting diode was powered to blink with a frequency corresponding to the fructose concentration in the berry. Also, power generation from blood sugar was demonstrated by inserting the needle into a rabbit vein. Such needle-based biofuel cells can be expected to serve in the future as the power unit of biodevices for environmental or healthcare monitoring.
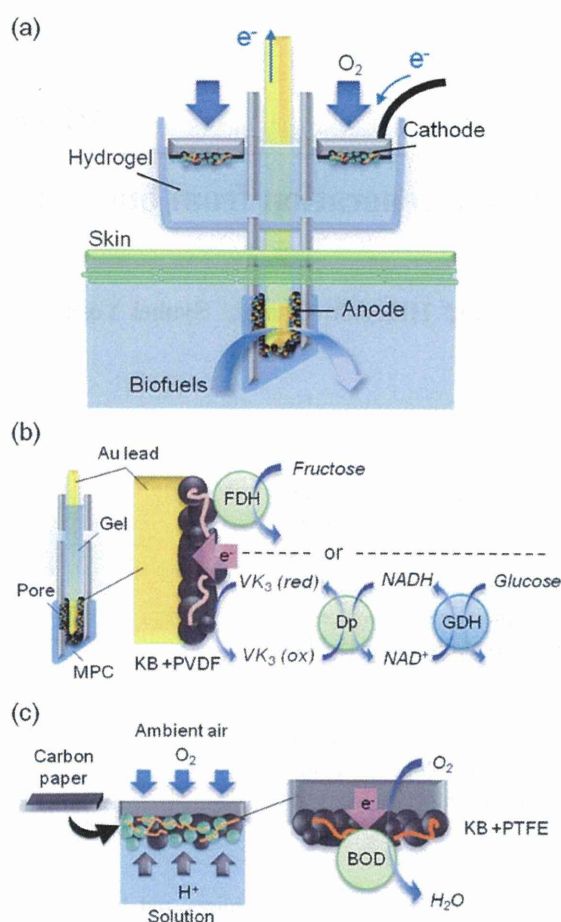
Fig. 1 (a) Schematic structure of a biofuel cell designed to utilize biochemical energy in living organisms. (b) Schemes of oxidation of fructose and glucose at the enzymatic needle anodes. (c) Schemes of O_2 reduction at the enzymatic gas-diffusion cathode.

bioanode for oxidation of fructose or glucose inside living organisms (Fig. 1b), and a carbon paper-based gas-diffusion biocathode for reduction of the abundant oxygen in the ambient air (Fig. 1c). This anode and cathode are assembled using an ion-conducting agarose hydrogel as the inner matrix. This novel structural design allows insertion into the organisms even through tough skins, and protects the cathode from reaction inhibitors present in the biofluids.

Experimental section

Fabrication of needle anodes

Both ends of an eppendorf plastic needle or one end of an SUS syringe (TERUMO, 25G) was cut as shown in Fig. S1†. The SUS needle was insulated by electrodeposition of anodic electrophoretic paint (ELECOAT AE-X, SHIMIZU, applied voltage: 10 V, deposition time: 3 min). After inserting gold wire into these needles, a 1% solution of agarose containing buffer salts (80 °C) is injected into the internal needle space and cooled in air. Since the hydrogel-filled needle blocks the subsequent injection of enzyme solutions, 1 mm diameter holes were drilled in the

sidewall of the needles to reduce the inner pressure. As we explain in the Results and discussion section, the holes act also as effective windows for fuel supply.

The anode for fructose oxidation was prepared using a plastic needle and fructose dehydrogenase (FDH, EC 1.1.99.11, 160 U) from *Gluconobacter*. 2 μl of a solution containing ketjenblack (KB)/poly(vinylidene fluoride) (PVDF) (3 : 1, 10 mg ml⁻¹) was coated on the gold wires (*ca.* 0.057 cm² geometric surface area). After drying in air, the electrode was modified with a 3 mg ml⁻¹ FDH solution, followed by drying in air.

An SUS needle was used for the anode for glucose oxidation with glucose dehydrogenase (GDH, EC 1.1.1.47, 250 U mg⁻¹) from *microorganism*, diaphorase (Dp, EC 1.6.99, 1000 U mg⁻¹) from *Clostridium*, Poly-L-Lysine-modified vitamin K₃ (PLL-VK₃) and nicotinamide adenine dinucleotide (PLL-NAD⁺) according to the protocol previously described.[19–22] 4 μl PLL-VK₃ solution (4.83 mM) was mixed with a 3 μl Dp solution (14 mg ml⁻¹), 1 μl poly(ethylene glycol) diglycidyl ether (PEGDE, 10 mg ml⁻¹) solution and 3 μl KB solution (20 mg ml⁻¹). A 2.5 μl aliquot of the mixed solution was put on a gold wire (*ca.* 0.0032 cm² geometric surface area) and dried in air. The surface of a PLL-VK₃/Dp/KB electrode was coated with 2.4 μl of a solution containing a 40 mg ml⁻¹ GDH solution, a 10 mg ml⁻¹ PLL solution and a 50 mg ml⁻¹ PLL-NAD⁺.

Preparation of gas-diffusion cathodes

A solution containing KB/poly(tetrafluoroethylene) (PTFE) (1 : 1, 8 mg ml⁻¹) was put on a 0.2 mm thick Toray carbon paper (CP) and dried in air. A 4 mm diameter hole was previously punched at the center of the CP. The surface of the KB-modified CP electrode was modified with a 5 mg ml⁻¹ solution of bilirubin oxidase (BOD, EC 1.3.3.5, 2.5 U mg⁻¹, from *Myrothecium*). After drying in air, the electrode was further coated with a mixed KB solution to make the surface hydrophobic. This enzyme-modified electrode was mounted on a chamber made from PDMS, which was filled with 1% agarose hydrogel containing buffer salts. The geometric surface area of the CP electrode was 0.67 cm² (the device for a grape) or 0.19 cm² (the device for a rabbit).

Electrochemical measurements

The anode and the cathode of the cell were connected through an analog-type variable resistor (range: from 2 MΩ to 28 Ω). The cell voltage and electrode potentials were measured against a homemade Ag|AgCl (saturated KCl) reference electrode by an electrochemical analyzer combined with LabVIEW (program: LabVIEW software, hardware for voltage detection: NI USB-6221) at given values of the resistance. The current and the power were derived from the detected cell voltage and the resistance.

The grape used is RED GLOBE (GROS COLMAN). *In vivo* measurements in the rabbits have been carried out in accordance with the guidelines of Tohoku University Environmental & Safety Committee (no. 22EgA-4). The rabbits were anesthetized with ketamine hydrochloride (35 mg kg⁻¹) and xylazine hydrochloride (5 mg kg⁻¹), awaking from anesthesia for 1 hour, by which time we would measure the cell voltage by inserting the anode of the cell into the ear veins of the rabbits.

Results and discussion

Performance of gas-diffusion biocathodes

Fig. 2a shows cyclic voltammograms of the gas-diffusion cathode at 10 mV s⁻¹. The carbon paper-based biocathodes were put on an oxygenic pH 7.0 buffer solution so as to contact the solution by the BOD-modified face (thin solid plot). The reduction current density reaches -0.5 mA cm⁻² at 0 V, a value of which is twice that of a biocathode that was entirely immersed in the solution (broken plot). Such superior performance of a gas-diffusion cathode originates in the efficient supply of oxygen from the ambient air through the carbon paper.[23–26] The oxygen solubility in water is limited to ~0.3 mM and its diffusion coefficient is also small (2×10^{-5} cm² s⁻¹). In contrast, these values in air are orders of magnitude larger, ca. 10 mM and 2×10^{-1} cm² s⁻¹. The performance of an O_2-diffusion biocathode can be further improved by modifying the three-phase interface, consisting of the current collecting solid phase (enzyme-modified electrode), the electrolyte solution liquid phase, and the gas phase for oxygen supply.[16,27] For example, an additional coating of hydrophobic KB onto the BOD-modified face of the biocathode was effective in controlling excess penetration of liquid (Fig. 2b), which led to a fourfold performance up to ca. -2 mA cm⁻² at 0 V (bold plot in Fig. 2a). This improved cathode will contribute to the miniaturization of the biofuel cell assembly as described later. Because the BOD enzyme shows activity over a wide pH range (pH 4–7), cathode performance of the same quality was observed even under acidic pH 5.0 conditions, as shown in Fig. S2†. Therefore, the present O_2-diffusion BOD cathode is applicable to experiments both of a grape with pH 5.0 gel and of a rabbit vein with pH 7.0 gel.
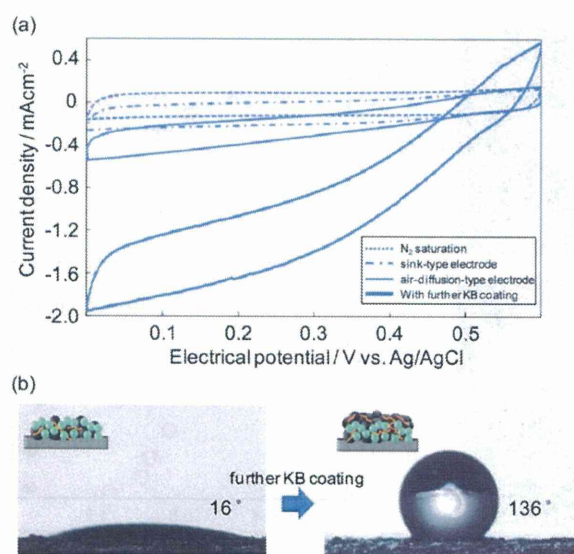

Fig. 2 (a) Cyclic voltammograms of O_2 reduction at BOD/KB (sink- and diffusion-type) and KB/BOD/KB (diffusion-type) electrodes at 10 mV s⁻¹. The control experiment in N_2-satuirated solution is also shown. (b) Photographs of water droplets placed on BOD/KB (contact angle = 16°) and KB/BOD/KB surfaces (contact angle = 136°).

Power generation from raw grapes

A biofuel cell device for fruits was constructed using the O_2-diffusion BOD cathode and the needle bioanode modified with FDH for fructose oxidation. These electrodes were mounted in a PDMS chamber filled with agarose hydrogel prepared with 750 mM McIlvaine buffer solution (pH 5.0). The device was inserted into a grape as shown in Fig. 3a, and at first the performance of the needle anode was evaluated using an externally inserted Ag/AgCl reference electrode (Fig. 3b). The needle anode without the side pore shows an oxidation current density of 0.35 mA cm⁻² (current: 20.1 μA, geometric electrode area: 0.057 cm²) at 0.6 V by oxidation of fructose that penetrated though the needle aperture. By opening the side pores, the anodic performance in a grape was enhanced up to 1.53 mA cm⁻² (current: 87.6 μA) at 0.6 V.

Fig. 3c shows the cell performance using a raw grape at room temperature. The upper panel shows the cell voltage, the anode potential and the cathode potential as functions of the cell current, while the lower panel shows the cell power. The device generated 6.3 μW of electrical power (111 μW cm⁻¹⁻²) with a cell current of 25 μA at 0.25 V (0.23 V anodic potential and 0.48 V cathodic potential vs. Ag/AgCl). The cell performance was strongly dependent on the concentration of the buffer in the agarose gel. For example, the device using 30 mM buffered gel produced only 2.2 μW. Importantly, the total performance could be amplified by connecting an array of needle anodes in parallel; the device with the array of four needle anodes (Fig. S3†) had a fourfold output power, ca. 26.5 μW (Fig. 3d).

The raw grape contains not only fructose but also glucose at a similar concentration.[28,29] However, the GDH-based needle anode modified for glucose oxidation did not work well in the grape (Fig. S4†) because the activity of GDH is lowered in acidic conditions.[19–22]

As the final experiment using grapes, we demonstrate the possibility of monitoring sugar levels in the fruit. A FDH-based needle biofuel cell was combined with an LED device consisting of a charge pump IC, a 1 μF ceramic capacitor and a red LED. As we reported previously,[30] the blink interval of the LED is inversely proportional to the power of the biofuel cell, which is roughly proportional to the concentration of the biofuel. In practice, the LED blinks at a higher frequency with an increase in the fructose concentration (Fig. 3e), and the concentration of fructose within the grape was estimated to be roughly 20–40 mM. In fact, the power curve in the 35 mM fructose experimental solution was almost identical with that in the grape, as shown in Fig. S5†.

Power generation from a rabbit ear vein

Power generation from blood requires biocompatibility in order to prevent the formation of a blood clot on the electrode surface. To make the electrode biocompatible, a coating with 2-methacryloyloxyethyl phosphorylcholine (MPC)-polymer[31] is effective. In fact, as shown in Fig. 4a, an MPC-treated substrate resisted blood clotting even after immersion in blood for 2 hours. Fig. 4b shows cyclic voltammograms of the MPC-coated or uncoated GDH/PLL-NAD⁺/Dp/PLL-VK₃ needle anodes in PBS solution containing 10 mM glucose. Both reached to current density of ca. 1.5 mA cm⁻² (current: 5.0 μA, geometric electrode
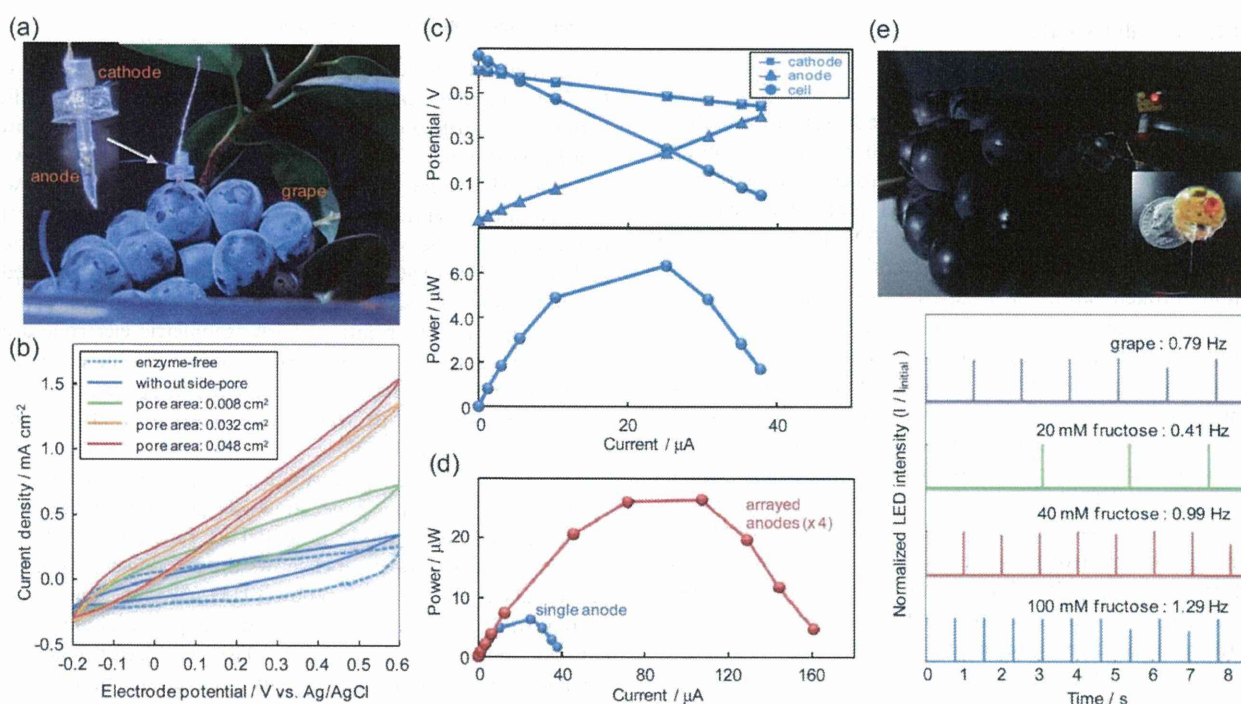
Fig. 3 (a) Photograph of the assembled biofuel cell inserted into a grape. (b) Cyclic voltammograms of FDH-modified needle anodes at 10 mV s^{-1} in a raw grape. Side pores were drilled in the wall of the needle (pore area: 0.008, 0.032 and 0.048 cm^2). (c) (upper panel) Polarization curve of the biofuel cell in the grape at room temperature. The cell voltage (●), the cathode potential vs. Ag/AgCl (■) and the anode potential vs. Ag/AgCl (▲) are plotted as function of the current density. (lower panel) Variation of the power with the cell current. (d) Power output of the biofuel cell using single anode and arrayed anodes (×4). (e) Monitoring of sugar level in a raw grape with a self-powered fructose-sensing devices. The device consists of the biofuel cell and an LED system, whose blink interval is correlated with the fructose concentration.
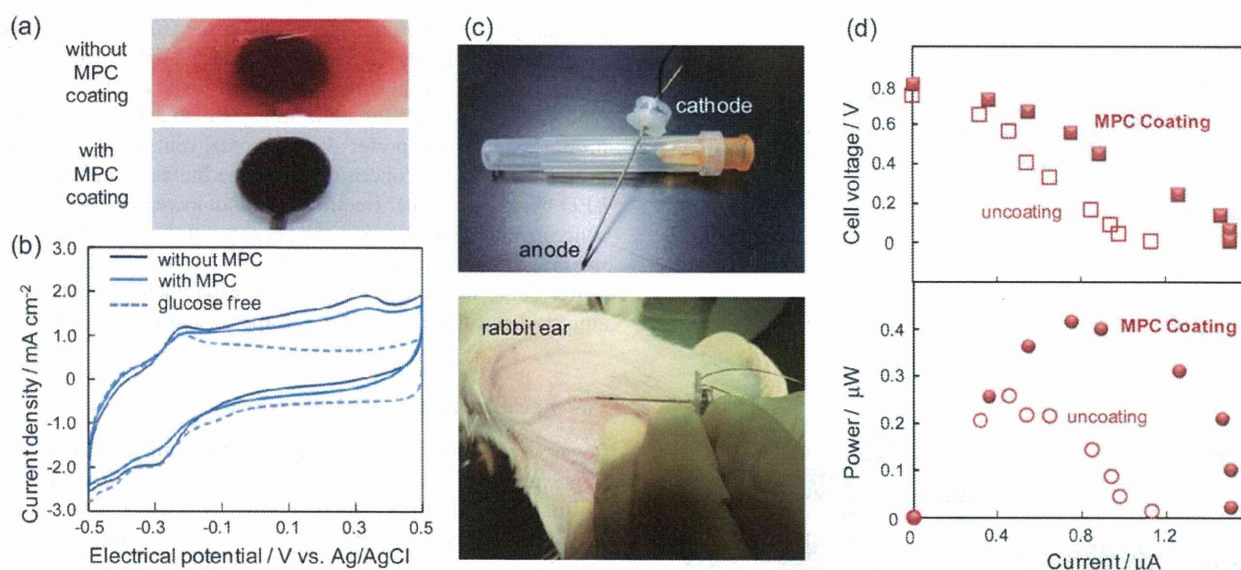
Fig. 4 (a) Photographs of electrode substrates with (and without) a MPC-coating, taken after soaking in withdrawn blood for 2 hours. (b) Cyclic voltammograms of bare and MPC-coated needle bioanodes at 10 mV s^{-1} in phosphate buffer containing 10 mM glucose. The control experiment (glucose-free) is also shown. The current density was estimated from the geometric area of the anode, 0.0032 cm^2. (c) Photographs of the assembled biofuel cell for power generation from a rabbit vein. (d) Performance of the biofuel cells using a needle anode, with and without MPC-coating, taken by inserting the needle anodes into a rabbit vein.

area: 0.0032 cm²) at 0.5 V with a CV shape corresponding to glucose oxidation at GDH/PLL-NAD⁺/Dp/PLL-VK₃ electrode.[19–21] These results indicate that the MPC coating serves as a bioinert layer without significant disturbance for the glucose transport to the enzyme electrodes inside the needle.

By assembling this needle anode with the O₂-diffusion BOD cathode, the fuel cell performance was evaluated by inserting it into a vein of a rabbit ear (Fig. 4c). Fig. 4d shows the typical current–voltage and current–power curves obtained by changing the external resistance (10 kΩ–2 MΩ). The open-circuit voltage of the cell was 0.81 V, which is similar to the difference between the potentials at which glucose oxidation and oxygen reduction start to occur in cyclic voltammograms (0.55 V in Fig. 2a and −0.30 V in Fig. 4b, respectively). The performance of the anode is reflected in the maximum cell current, 1.50 μA (466 μA cm⁻²). The power for this cell reached 0.42 μW at 0.56 V, while the device without a MPC coating showed ~40% loss in power. Since the MPC coating has no significant effect on the electrode processes (Fig. 4b), the lowered performance is probably due to the formation of blood clots. In fact, after the insertion experiment, the formation of some biofilms was observed only on the needle anodes without the MPC coating. Probably, the blood clots interfere with the transport of glucose into the needle, and may also have effects on the cell resistance and kinetics.

Conclusions

We assembled a biofuel cell with a needle anode and gas-diffusion cathode, as a practical form of cell for direct power generation from natural organisms with skins. The results presented here include techniques to improve the performance of the devices. (1) A gas-diffusion cathode treated to be hydrophobic showed higher activity. (2) Incorporating side pores into the needles effectively enhanced the supply of biofluids to the inner anodes. (3) Modification of the needle tip with MPC polymer was required to obtain comparatively stable power from bloods. We also demonstrated that an array of needle anodes led to an increase in the output power (Fig. 3d). In the near future, a finer array of microscopic needle anodes will be fabricated by advanced micro-/nano-techniques for realizing a minimally invasive patchable biofuel cell system.

Acknowledgements

References

1 I. Willner, E. Katz, Bioelectronics, Wiley-VCH, Weinheim, 2005.
2 G. T. R. Palmore, H. Bertschy, S. H. Bergens and G. M. Whitesides, J. Electroanal. Chem., 1998, 443, 155.
3 I. Willner, Y. M. Yan, B. Willner and R. T. Vered, Fuel Cells, 2009, 1, 7.
4 M. J. Moehlenbrock and S. D. Minteer, Chem. Soc. Rev., 2008, 37, 1188.
5 W. Gellett, M. Kesmez, J. Schumacher, N. Akers and S. D. Minteer, Electroanalysis, 2010, 7-8, 727.
6 A. Heller and B. Feldman, Chem. Rev., 2008, 108, 2482.
7 S. C. Barton, J. Gallaway and P. Atanassov, Chem. Rev., 2004, 104, 4867.
8 J. A. Cracknell, K. A. Vincent and F. A. Armstrong, Chem. Rev., 2008, 108, 2461.
9 J. Wang, Talanta, 2008, 75, 636.
10 Y. Liu and S. Dong, Biosens. Bioelectron., 2007, 23, 593.
11 D. Wen, X. Xu and S. Dong, Energy Environ. Sci., 2011, 4, 1358.
12 N. Mano, F. Mao and A. Heller, J. Am. Chem. Soc., 2003, 125, 6588.
13 N. Mano, H. H. Kim, Y. Zhang and A. Heller, J. Am. Chem. Soc., 2002, 124, 6480.
14 S. Shleev, G. Shumakovich, O. Morozova and A. Yaropolov, Fuel Cells, 2010, 4, 726.
15 X. Li, L. Zhang, L. Su, T. Ohsaka and L. Mao, Fuel Cells, 2009, 1, 85.
16 C. Kang, H. Shin, Y. Zhang and A. Heller, Bioelectrochemistry, 2004, 65, 82.
17 C. Kang, H. Shin and A. Heller, Bioelectrochemistry, 2006, 68, 22.
18 P. Rowinski, C. Kang, H. Shin and A. Heller, Anal. Chem., 2007, 79, 269.
19 F. Sato, M. Togo, M. K. Islam, T. Matsue, J. Kosuge, N. Fukasaku, S. Kurosawa and M. Nishizawa, Electrochem. Commun., 2005, 7, 643.
20 M. Togo, A. Takamura, T. Asai, H. Kaji and M. Nishizawa, Electrochim. Acta, 2007, 52, 4669.
21 M. Togo, A. Takamura, T. Asai, H. Kaji and M. Nishizawa, J. Power Sources, 2008, 178, 53.
22 T. Miyake, M. Oike, S. Yoshino, Y. Yatagawa, K. Haneda and M. Nishizawa, Lab Chip, 2010, 10, 2574.
23 G. Gupta, C. Lau, V. Rajendran, F. Colon, B. Branch, D. Ivnitski and P. Atanassov, Electrochem. Commun., 2011, 4, 247.
24 X. Wu, F. Zhao, J. R. Varcoe, A. E. Thumser, C. A. Rossa and R. C. T. Slade, Biosens. Bioelectron., 2009, 24, 326.
25 A. Habrioux, G. Merle, K. Servat, K. B. Kokoh, C. Innocent, M. Cretin and S. Tingry, J. Electroanal. Chem., 2008, 579, 97.
26 G. Gupta, C. Lau, B. Branch, V. Rajendran, D. Ivnitski and P. Atanassov, Electrochim. Acta, 2011, DOI: 10.1016/j.electacta.2011.01.089.
27 R. Kontani, S. Tsujimura and K. Kano, Bioelectrochemistry, 2009, 76, 10.
28 W. M. Kliewer, Am. J. Enol. Vitic., 1967, 18, 33.
29 J. K. Palmer and W. B. Brandes, J. Agric. Food Chem., 1974, 22, 709.
30 T. Miyake, S. Yoshino, T. Yamada, K. Hata and M. Nishizawa, J. Am. Chem. Soc., 2011, 133, 5129.
31 K. Ishihara, T. Ueda and N. Nakabayashi, Polym. J., 1990, 22, 355.

Tumor Necrosis Factor-α Mediates Photoreceptor Death in a Rodent Model of Retinal Detachment

Toru Nakazawa,[*,1,2] *Maki Kayama,*[2] *Morin Ryu,*[1] *Hiroshi Kunikata,*[1] *Ryou Watanabe,*[1] *Masayuki Yasuda,*[1] *Jiro Kinugawa,*[1] *Demetrios Vavvas,*[2] *and Joan W. Miller*[*,2]

Purpose. Photoreceptor degeneration is a major cause of visual loss in various retinal diseases, including retinal detachment (RD) and neovascular AMD, but the underlying mechanisms remain elusive. In this study, the role of TNFα in RD-induced photoreceptor degeneration was investigated.

Methods. RD was induced by subretinal injection of hyaluronic acid. Photoreceptor degeneration was assessed by counting the number of apoptotic cells with TdT-dUTP terminal nick-end labeling (TUNEL) 3 days after RD and measurement of the outer nuclear layer (ONL) thickness 7 days after RD. As the target of anti-inflammatory treatment, the expression of TNFα, with or without dexamethasone (DEX) was examined in rats by real-time PCR. To understand the role of TNFα in photoreceptor degeneration, RD was induced in mice deficient in TNFα or its receptors (TNFR1, TNFR2, and TNFR1 and -2), or in wild-type (WT) mice by using a functionally blocking antibody to TNFα. CD11b^{+} cells in the outer plexiform layer (OPL) and subretinal space were counted by immunohistochemistry (IHC).

Results. Treatment with DEX ($P = 0.001$) significantly suppressed RD-induced photoreceptor degeneration and the expression of TNFα. RD-induced photoreceptor degeneration was significantly suppressed with specific blockade of TNFα ($P = 0.032$), in mice deficient for TNFα ($P < 0.001$), TNFR2 ($P = 0.001$), or TNFR1 and -2 ($P < 0.001$). However, lack of TNFR1 did not protect against RD-induced photoreceptor degeneration ($P = 0.060$). Müller cell activation was unchanged in WT and TNFα^{−/−} mice. Recruitment of CD11b^{+} monocytes was significantly lower in the TNFα^{−/−} mice compared to WT mice ($P = 0.002$).

Conclusions. TNFα plays a critical role in RD-induced photoreceptor degeneration. This pathway may become an important target in the prevention of RD-induced photoreceptor degeneration. (*Invest Ophthalmol Vis Sci.* 2011;52:1384–1391) DOI:10.1167/iovs.10-6509

Photoreceptors are vulnerable in several retinal disorders, including macular degeneration,[1] retinal detachment (RD),[2–4] diabetic retinopathy,[5] retinopathy of prematurity,[6] and retinitis pigmentosa.[7] In these pathologic conditions, photoreceptors undergo apoptosis.[2,5–7] Therefore, new insights about the mechanisms that underlie photoreceptor degeneration in the ocular diseases would be of clinical interest and could lead to new neuroprotective treatments. Previously, we used the rodent model of RD to clarify the mechanism of RD-induced photoreceptor degeneration. We found that RD-induced photoreceptor apoptosis went through a caspase-dependent[8,9] or caspase-independent pathway.[10] Furthermore, we found that monocytes recruited through the upregulation of monocyte chemoattractant protein (MCP)-1 in Müller glial cells play a neurodestructive role in photoreceptor degeneration.[11,12]

Tumor necrosis factor (TNF)-α is synthesized, mainly in monocytes, as a 26-kDa precursor[13] that is cleaved proteolytically and secreted as a 17-kDa protein.[14] TNFα acts via either the low-affinity TNF receptor (TNFR1) or high-affinity TNF receptor (TNFR2).[15] TNFα is upregulated in several neurodegenerative disorders including multiple sclerosis, Parkinson's disease, and Alzheimer's disease and suppression of TNFα has demonstrated therapeutic effects.[16] In ophthalmic disorders, the vitreous samples from patients with RD contain significantly higher levels of TNFα than samples from patients with other retinal conditions, such as macular hole or idiopathic premacular fibrosis.[17,18] However, the role of RD-induced elevated TNFα on photoreceptor degeneration remains unclear.

Recently, TNFα-suppressing monoclonal antibodies such as infliximab have been successfully used to treat patients with inflammatory ocular disease, including Behçet's disease,[19] diffuse subretinal fibrosis (DSF) syndrome,[20] posterior scleritis,[21] retinal vascular tumors,[22] and neovascular age-related macular degeneration.[23] Thus, if TNFα plays a neurodestructive role in RD-induced photoreceptor degeneration, anti-TNFα treatment may be a good candidate for neuroprotective treatment in retinal diseases. In this study, we induced RD in mice deficient in TNF, TNFR1, and TNFR2 and investigated the role of the TNFα pathway on RD-induced photoreceptor apoptosis.

MATERIALS AND METHODS

Animals

All animal procedures were performed in accordance with the ARVO Statement for the use of Animals in Ophthalmic and Vision Research and the National Institute of Health Guidance for the Care and Use of

Laboratory Animals. The protocol was approved by the Animal Care Committee of the Massachusetts Eye and Ear Infirmary and by the Ethics Committee for Animal Experiments of Tohoku University Graduate School of Medicine.

Adult male Brown-Norway rats, TNFα-deficient mice (TNFα$^{-/-}$), TNF receptor 1 and -2 double-deficient mice (TNFR$^{-/-}$; B6.129SF2J background, 20–25 g; Jackson Laboratory, Bar Harbor, ME), TNFR1-deficient mice (TNFR1$^{-/-}$, C57BL6 background; Jackson Laboratory), TNFR2-deficient mice (TNFR2$^{-/-}$, C57BL6 background; Jackson Laboratory), and age- and sex-matched B6.129SF2J mice or C57BL6 mice (wild-type [WT]) were housed in covered cages. Rats and mice were fed with standard rodent diet ad libitum and kept on a 12-hour light (250 lux)–dark cycle.

Surgical Induction of RD

RD was induced in rats and mice, as previously described.[11,12,24] Briefly, anesthesia was preformed with a mixture of xylazine hydrochloride (mice, 10 mg/kg; rats, 20 mg/kg) and ketamine hydrochloride (100 mg/kg). The pupils were dilated and a sclerotomy was created approximately 1 mm posterior to the limbus with a 30-gauge needle. A Glaser subretinal injector (20-gauge shaft with a 32-gauge tip; BD Biosciences, San Diego, CA) connected to a syringe filled with sodium hyaluronate (HealonGV; Pharmacia and Upjohn Co., Kalamazoo, MI) was then introduced into the vitreous cavity. A retinotomy was created in the peripheral retina with the tip of the subretinal injector, and 2 μL of sodium hyaluronate was slowly injected into the subretinal space (SRS), causing detachment of one half of the retina. One hour before RD, dexamethasone (DEX 1 mg/kg; Sigma-Aldrich, St. Louis, MO) or vehicle was injected intraperitoneally (IP). DEX was first dissolved in 100% ethanol alcohol to 1 mg/mL and then diluted in Dulbecco's phosphated-buffered saline (DPBS) to 0.5 mg/mL. Fifty percent ethanol alcohol in DPBS was used as a vehicle control. To block the TNFα in rat RD, the blocking antibody for TNFα was used (goat anti-rat TNFα, 0.1 μg/μL; R&D Systems, Minneapolis, MN), and goat normal IgG (NGS, 0.1 μg/μL, azide free; R&D Systems) was the control. TNFα blocking antibody 1 μL was injected subretinally RD with a syringe (Hamilton, Reno, NV) equipped with a 32-gauge needle by introducing the tip of needle through the sclerotomy into the SRS and then injecting solution over 3 minutes. RDs were created only in the right eye of each animal, with the left eye serving as the control.

The activities of caspase-8 were measured according to the manufacturer's instruction in a commercially available kit (cat. no. APT171; Millipore, Billerica, MA). The retinal samples (150 μg) were harvested 1 to 3 days after the induction of RD, and these were treated with the vehicle, control IgG (1 μg/mL, 705-035-003; Jackson ImmunoResearch Products, West Grove, PA), and the blocking antibody for TNFα (1 μg/mL, goat IgG, cat. no. AB410-NA; R&D Systems) in mice (8 weeks).

Quantification of TUNEL$^+$ Photoreceptor In Vivo

To assess photoreceptor cell loss and apoptosis quantitatively, we used two methods as previously reported: measurement of the outer nuclear layer (ONL) thickness stained by hematoxylin-eosin (H-E) at 7 days after RD[11] and cell counting with TdT-dUTP terminal nick-end labeling (TUNEL; ApopTag Fluorescein In Situ Apoptosis detection kit S7110; Chemicon International, Inc., Temecula, CA) at 3 days after RD.[11] The number of TUNEL$^+$ cells was counted in a masked fashion. The area of the ONL was measured in the captured images (OpenLab software; Improvision Inc., Lexington, MA), and the cell count per square millimeter calculated.

RNA Extraction and RT-PCR

Total RNA extraction and quantitative RT-PCR was performed as previously reported.[11,12,24] Briefly, total RNA was extracted (RNA Purification System; Invitrogen, Carlsbad, CA) and 3 μm of total RNA was subjected to RT (SuperScript III First-Strand Synthesis System; Invitrogen). First strand cDNAs were amplified using a real-time PCR thermal cycler (ABI7700; Applied Biosystems, Inc. [ABI], Foster City, CA) with a

PCR core kit (SYBER Green; Applied Biosystems). The primer sets used in this study were as follows: IL-1β forward- TCAGGAAGGCAGTGTCACT-CATTG and reverse- ACACACTAGCAGGTCGTCATCATC; TNF-α forward-CCCAGACCCTCACACTCAGATCAT and reverse- GCAGCCTTGTCCCTT-GAAGAGAA; and MCP-1 forward- ATGCAGGTCTCTGTCACGCTTCTG, reverse- GACACCTGCTGCTGGTGATTCTCTT, all of which are described in another publication.[12] For relative comparison of each gene, we analyzed the Ct value of the real-time PCR data with the $^{\Delta\Delta}$Ct method, according to the manufacturer's instructions (ABI). To normalize the amount of sample cDNA added to each reaction, the Ct value of the endogenous control (18rRNA) was subtracted from the Ct value of each target gene.

Adult Mouse Retinal Primary Cultures

Adult primary retinal cultures were prepared as described elsewhere.[11] Briefly, isolated neural retinas were incubated at 37°C for 20 minutes in a CO_2 incubator in a digestion solution containing papain (10 U/mL; Worthington, Lakewood, NJ). Cell density was adjusted to 4.0×10^5 cells each well with neuronal cell growth medium (Neurobasal A, containing B27 supplement, NBA/B27; Invitrogen) and 1 μg/mL insulin, 2 mM L-glutamate, and 12 μg/mL gentamicin. One hour later, TNFα was added to culture medium to reach final concentrations (0.001, 0.01, and 0.1 ng/mL) and cells were incubated for further 24 hours. To assess the viability of photoreceptors, we performed immunocytochemistry (ICC) with rabbit anti-recoverin antibody (1:500 dilution, AB5585; Chemicon), as published.[11] The number of recoverin$^+$ photoreceptors was counted at 10 random fields per well with a fluorescence microscope (×20 objective) equipped with an imaging system, and the number of recoverin$^+$ cells was counted in a blind fashion with ImageJ software (developed by Wayne Rasband, National Institutes of Health, Bethesda, MD; available at http://rsb.info.nih.gov/ij/index.html). Values are given as the mean ± SEM of counts in four replicate wells.
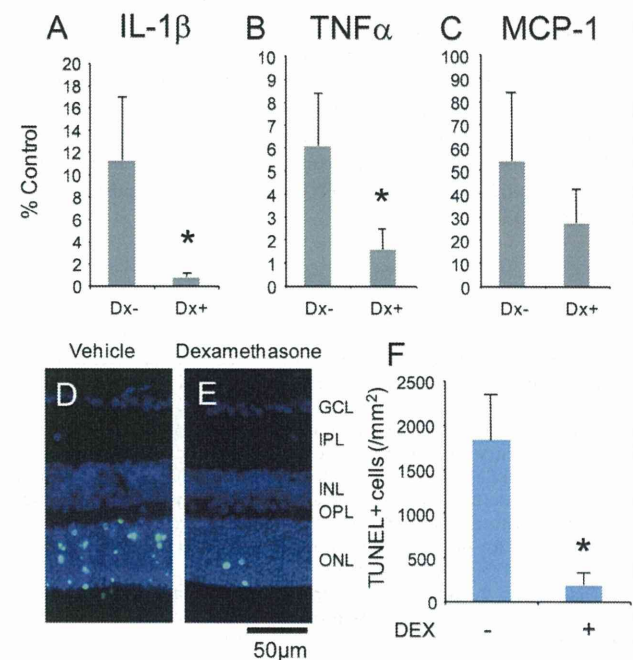

Figure 1. DEX suppresses the expression of cytokines and RD-induced TUNEL$^-$ photoreceptors in rats. (**A–C**) Quantitative real-time PCR data for IL-1β (**A**), TNFα (**B**), and MCP-1 (**C**) mRNA 1 hour after RD ($n = 6$). (**D–E**) Representative photography of detached retina labeled by TNUEL with (**E**) or without (**D**) DEX Quantification of TUNEL$^+$ photoreceptors 72 hours after RD with (+) or without (–) DEX (**F**). *Green*: TUNEL; *blue*: DAPI nuclear staining. *$P < 0.5$, treated versus untreated condition ($n = 6$ each). GLC, ganglion cell layer; IPL, inner plexiform layer.
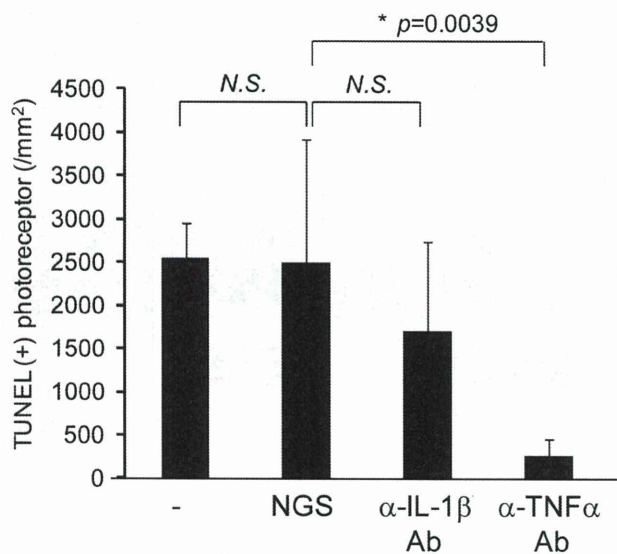
FIGURE 2.   A TNFα-blocking antibody prevents RD-induced photoreceptor loss 72 hours after RD in rats. Data are the number of TUNEL⁺ photoreceptors 72 hours after RD with subretinal administration of α-IL-1β antibody and α-TNFα antibody. NGS, normal goat serum.

Immunohistochemistry

Immunohistochemistry was performed as previously reported.[11,12,24] Briefly, 10-μm retinal sections through the optic nerve head were prepared and subjected to reaction with primary antibodies against phosphorylated ERK (pERK, 1:200; Cell Signaling Technology Inc., Beverly, MA), c-Fos (1:200; Santa Cruz Biotechnology, Inc., Santa Cruz, CA), or CD11b (1:200; Serotec Inc., Raleigh, NC). Retinal sections incubated with a buffer without the primary antibodies were used as negative controls. Fluorescence-conjugated secondary antibodies, including goat anti-mouse immunoglobulin G (IgG) and anti-rabbit IgG and anti-rat IgG conjugated to Alexa Fluor 488 (Molecular Probes, Eugene, OR) were used. Retinal sections were mounted with antifade medium (Vectashield; Vector Laboratories, Burlingame, CA) containing 4′,6 diamidino-2-phenylindole (DAPI) to reveal the nuclear structure. Immunolabeled cells were counted in photomicrographs of the center of the detached retinal area by using a microscope equipped with fluorescence illumination (DMRXA; Leica, Bannockburn, IL) and were analyzed (OpenLab software, ver. 2.2.5; Improvision). The pERK⁺, c-Fos⁺, and CD11b⁺ cells (at ×200 magnification) were counted in a masked fashion.

Statistical Analysis

The statistical significance of the RT-PCR result was determined with the Mann-Whitney U test. The data from the TUNEL and in vitro survival assays were analyzed with the Scheffé post hoc test (StatView 4.11J software for Macintosh; Abacus Concepts, Inc., Berkeley, CA). The significance level was set at $P < 0.05$. The data represent the mean ± SD except for culture results.

RESULTS

Anti-inflammatory Treatment with DEX Suppress the Photoreceptor Death and the Upregulation of TNFα Expression after RD

Previously, we showed that the expression of IL-1β, TNFα, and MCP-1 increased significantly after RD in rats.[12] In the present study, we first investigated the anti-inflammatory effect of the IP-DEX (1 mg/kg) on RD-induced photoreceptor degeneration in rats. This concentration of DEX was chosen because it

resulted in a neuroprotective effect on photoreceptors after photodynamic therapy (PDT) in our previous studies.[25] IP-DEX suppressed the RD-induced upregulation of IL-1β expression ($P = 0.004$; Fig. 1A) and TNFα expression ($P = 0.006$; Fig. 1B) 1 hour after RD ($n = 6$), and MCP-1 also showed a trend toward suppression ($P = 0.055$; Fig. 1C). We next investigated whether the IP-DEX anti-inflammatory effect resulted in neuroprotection for the RD-induced photoreceptor degeneration. IP-DEX significantly suppressed the RD-induced photoreceptor degeneration ($n = 9$, $P = 0.0005$; Figs. 1D–F). To examine the role of IL-1β and TNFα on photoreceptor degeneration, we injected anti-IL-1β or anti-TNFα neutralizing antibody subretinally and counted TUNEL⁺ cells in the ONL 3 days after RD in rats. We found that anti-TNFα antibody significantly decreased the number of TUNEL⁺ photoreceptors ($P = 0.004$), but anti-IL-1β antibody did not ($P = 0.109$) compared with the effect of normal goat IgG (Fig. 2). These data demonstrate that anti-inflammatory treatment with DEX and anti-TNFα blocking antibody has a significant neuroprotective effect on the RD-induced photoreceptor degeneration.

Cytotoxic Effect of TNFα on Cultured Photoreceptors

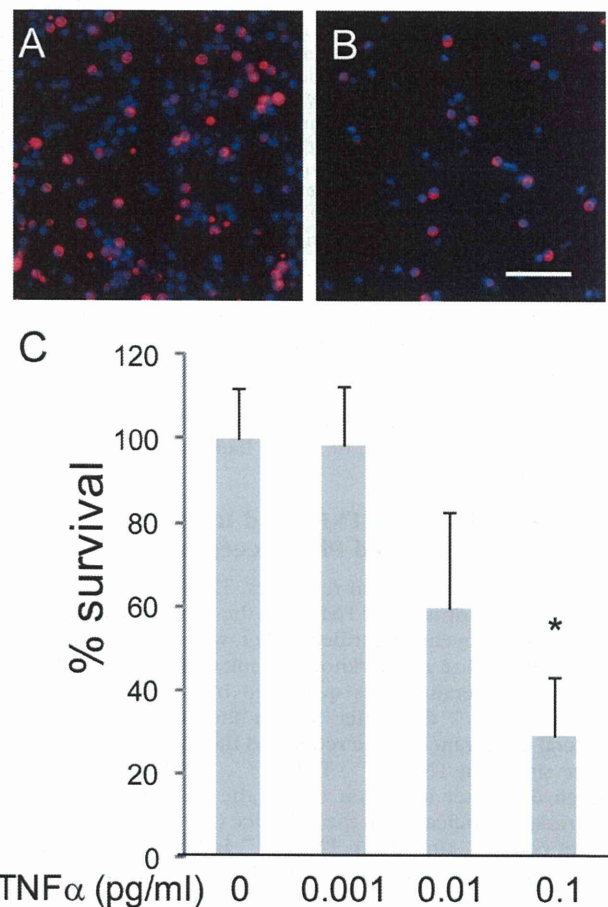To investigate the roles of the increased expression of TNFα after RD, we administered TNFα on cultured photoreceptors

FIGURE 3.   Cytotoxicity of TNFα for adult cultivated photoreceptors. (A, B) Recoverin⁺ photoreceptors in culture with (B) or without (A) TNFα. Red: recoverin⁺ photoreceptors; blue: DAPI nuclear staining. Scale bar, 100 μm. (C) Dose–response effects of TNFα cytotoxicity on recoverin⁺ photoreceptors. *$P < 0.05$ compared with controls without TNFα.